PSFC/JA-04-29

ICRF loading studies on Alcator C-Mod

A. Parisot, S. J. Wukitch, P. T. Bonoli, J.W. Hughes,
B. Labombard, Y. Lin, R. Parker, M. Porkolab, A.K. Ram

September 2004

Plasma Science and Fusion Center
Massachusetts Institute of Technology
Cambridge MA 02139 USA

This work was supported by the U.S. Department of Energy, Cooperative Agreement No. DE-FC02-99-ER54512. Reproduction, translation, publication, use and disposal, in whole or in part, by or for the United States government is permitted.

Submitted for publication to *Plasma Physics and Controlled Fusion.*

ICRF loading studies on Alcator C-Mod

A. Parisot, S.J. Wukitch, P. Bonoli, J.W. Hughes, B. LaBombard, Y. Lin, R. Parker, M. Porkolab, A.K. Ram

Plasma Science and Fusion Center, MIT, Cambridge MA 02139 USA

Abstract. Rapid changes in the loading resistance of fast wave antennas can limit high power operations of heating systems in the Ion Cyclotron Range of Frequencies (ICRF). Although novel matching techniques are being developed to reduce their effects, understanding the physics involved in these variations is of interest to guide and facilitate the design effort. We have studied the dependence of the loading resistance upon plasma parameters for the three ICRF antennas in the Alcator C-Mod tokamak. In contrast with similar studies in JET and Tore Supra, the evanescent decay term was not found to play an important role. The dominant variations could be related to changes in the shape of the electron density profiles in the propagating region. In H-mode, the loading resistance decreases as the density at the top of the pedestal is increased, and increases for higher Scrape-Off Layer densities. This dependency on global plasma parameters is generally identical for the three antennas, up to a proportionality constant, while local changes in front of an individual antennas could explain the residual discrepancy. To link the observations with theory, the surface impedance at the Faraday shield was calculated by solving the wave equation in a slab geometry using experimental radial density profiles. This approach leads to a good agreement with measurements over a wide range of operating conditions in L-mode, ELM-free and EDA H-mode plasmas, and it can be interpreted qualitatively in terms of impedance transformation in the scrape-off layer region. Implications for more complex modeling approaches are also discussed.

E-mail: `parisot@mit.edu`

1. Introduction

In the Ion Cyclotron Range of Frequencies (ICRF), flexible and efficient heating schemes can be obtained using fast magnetosonic waves (FW) launched from the plasma edge [Porkolab et al.(1998)]. A well-known constraint is the limited accessibility of the resonance and mode conversion layers due to the evanescent region at the edge. As a result, FW antennas are characterized by a low loading resistance and impedance matching techniques must be used. Traditional matching systems have proved relatively successful for this task and significant heating power has been coupled in severals tokamaks like JET (22 MW, [Kaye(94)]) and Tore Supra (10 MW, [M. Goniche and Colas(2003)]). While some issues remain, ICRF schemes are now widely seen as a viable auxiliary heating technique for next-step tokamak experiments and reactors.

Among the remaining limitations, the coupling of FW still imposes large restrictions on performance and flexibility. The loading impedance can experience significant and rapid variations as the plasma parameters are changed or evolve during a discharge. As this happens, traditional tuning systems cannot maintain matched conditions. The generator efficiency is then reduced. For a given heating power, higher voltages can also be encountered in the transmission components and trigger breakdown. While novel impedance matching solutions [Pinsker(1998)] are being investigated to increase these operation limits for given loading behaviors, understanding the physics of ICRF wave coupling and developing predictive tools for loading variations in various regimes could facilitate and guide this effort.

Numerical codes are one possible approach to confirm physical models and provide directions for antenna and matching system design. The effort in this direction has been progressing rapidly with modeling tools like RANT3D [Carter et al.(1996)], ICANT [Pécoul et al.(1998)] and TOPICA [Maggiora et al.(2003)], but as yet, the required robustness and accuracy for reliable predictions of the loading in plasma conditions has not been demonstrated. To study or characterize the effect of plasma parameters, such level of modelling detail is also not completely necessary, and simpler approaches can often provide useful physical insight.

For instance, one can analyze dominant effects experimentally or derive scaling laws for the loading resistance of different antennas, using experimental databases. The approach is always semi-empirical, as the functional dependence is chosen according to dominant factors predicted by the theory. Such investigations have been recently conducted in DIII-D [Mayberry et al.(1990)], JET [Hartmann et al.(2001)] and Tore Supra [M. Goniche and Colas(2003), Clairet(2002)].

In this paper, we report results from a study of the ICRF loading on the Alcator C-Mod tokamak using a similar approach. With its three antennas and operation at high field and high density, the device (presented in Sec. 2) offers interesting characteristics regarding ICRF coupling studies. The evanescent length does not change significantly in C-Mod and should not lead to large loading variations, according to ICRF coupling theories developed in earlier studies (Sec. 3). This contrasts with dominant trends in JET, Tore Supra and DIII-D. Experimentally, the loading is relatively unaffected by the outer gap, but changes significantly

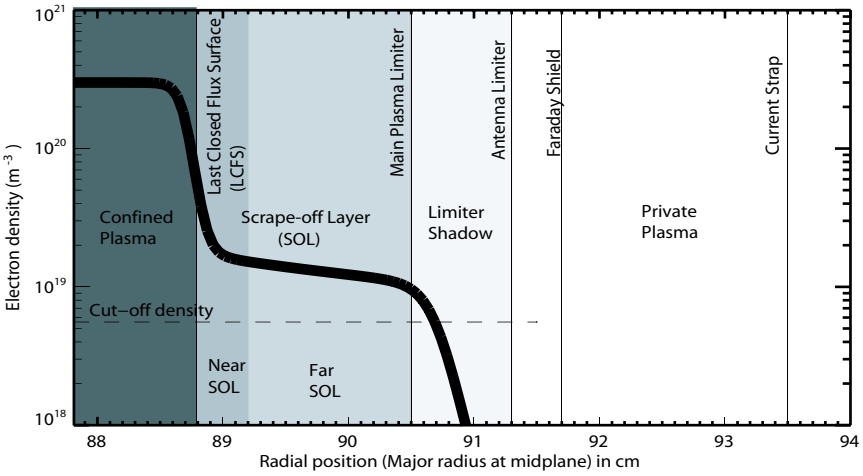

Figure 1. Typical radial density profile in C-Mod and radial position of the antenna components at the midplane.

as the density profi le evolves in the propagating region (Sec. 4). The observed dependence can be explained by a simple model of wave propagation at the edge and interpreted in terms of impedance transformation (Sec. 5). Deviations from the model are studied and could be related to local changes in plasma conditions in front of the antennas (Sec. 6).

2. ICRF system and density profile measurements in Alcator C-Mod

The Alcator C-Mod tokamak is a compact, high density (up to $10^{21}m^{-3}$) and high toroidal fi eld (up to 8.1 T) device, equipped with three ICRF antennas [Wukitch et al.(2002)]. Two two-strap center-grounded antennas at the D and E horizontal ports are operated at 80 and 80.5 MHz respectively, and up to 1.5 MW each. A compact four-strap antenna is installed at J-port and has been used to couple up to 3 MW at 70 and 78 MHz. J-antenna uses end-grounded straps with a folded structure, but the strap length is identical for all three antennas (44 cm). The strap to strap distance on center is 25.75 cm for D and E (peak $k_{||} \approx 10m^{-1}$ for $0 - \pi$ phasing), and 18.6 cm for J (peak $k_{||} \approx 14m^{-1}$ for $0 - \pi - 0 - \pi$ phasing). C-Mod has a major radius of $\approx$ 67 cm and a typical minor radius of 22 cm. Figure 1 shows the radial position of the different antenna components at the midplane and a typical density profi le. The results presented here correspond to the D(H) scheme, i.e. deuterium plasmas with hydrogen minority heating at its fundamental resonance (hydrogen concentration $< 10\%$). This scenario leads to strong single pass absorption [Porkolab et al.(1998)] (over 70% for typical plasmas parameters).

The coupling to the plasma is evaluated for each discharge using a directional coupler

located between the impedance matching system and the antennas. Of particular interest is the loading resistance R_L, which is obtained from $P_{net} = \frac{V_{max}^2}{2}\frac{R_L}{Z_0^2}$, where P_{net} is the net power in the transmission line feeding the antenna system, V_{max} the voltage at high voltage points and Z_0 is its characteristic impedance. Measurements presented here correspond to a pair of two radiating straps, allowing the two and four strap antennas to be compared directly.

The radial density profile at the edge is measured routinely in C-Mod using a Thomson Scattering diagnostic [Hughes et al.(2001), Hughes et al.(2003)]. Its range extends down to $n_e = 0.3 \times 10^{20} m^{-3}$ with a radial resolution of 1.3 mm at the midplane. The density profile in the Scrape-Off Layer (SOL) is measured using a fast scanning Langmuir probe. The data is only available for discharges with low ICRF power input, due to heat loads and RF electric field pickup in high RF power discharges. In the absence of probe measurements, the neutral pressure at the outboard midplane can still provide some information on the SOL conditions. Typical radial profiles in L-mode and H-mode are shown on Figure 2. The ELM-free H-mode regime is characterized by the formation of a transport barrier at the edge of the plasma and a decreased density in the SOL. In the Enhanced D-Alpha (EDA) H-mode regime [Greenwald et al.(1999)], the density pedestal is still present, but the density in the scrape-off layer is higher. The evolution of the density profile occurs on timescales as short as 100 μs.

3. ICRF coupling theory and the Alcator C-Mod regime

As reported in Mayberry et al. [Mayberry et al.(1990)], the evolution of the edge density profile can affect the ICRF loading resistance significantly. The authors proposed two possible mechanisms:

A. Changes in the evanescent length (distance to cutoff) As can be seen from its dispersion relation, the fast wave launched at an angle is not propagating below a given density $n_{e,cutoff}$ called *cutoff density* and defined by the condition $n_\parallel^2 = R \equiv 1 - \sum_j \frac{\omega_{pj}^2}{\omega(\omega+\Omega_{cj})}$ [Stix(1992)] where j denotes the different ion species and ω_p, Ω_c respectively the plasma and cyclotron frequencies. The accessibility of the FW depends strongly on the length L of the evanescent region between the antenna straps and the cutoff layer where this density is reached. As the density in the SOL is reduced in ELM-free H-mode, the cutoff moves away from the antenna and therefore the coupling is reduced. A simple model treats the evanescent region as vacuum, with the wavenumber in the radial direction $k_x^2 = \frac{\omega^2}{c^2} - k_\parallel^2 \approx -k_\parallel^2$ and leads to $R_L \propto \exp(-2k_\parallel L)$.

B. Density gradient at the edge Theoretical calculations based on a linear density profile [Vdovin(1983)] suggest that a higher density gradient at the edge leads to lower loading. The formation of a density pedestal during H-mode creates a region with strong density gradient and leads to an additional decrease in the loading resistance compared to that expected from the changes in the evanescent length only.

Although Mayberry et al. indicated that the two possible mechanisms could be equally important, the distance to cutoff is usually observed to be the dominant factor, as in

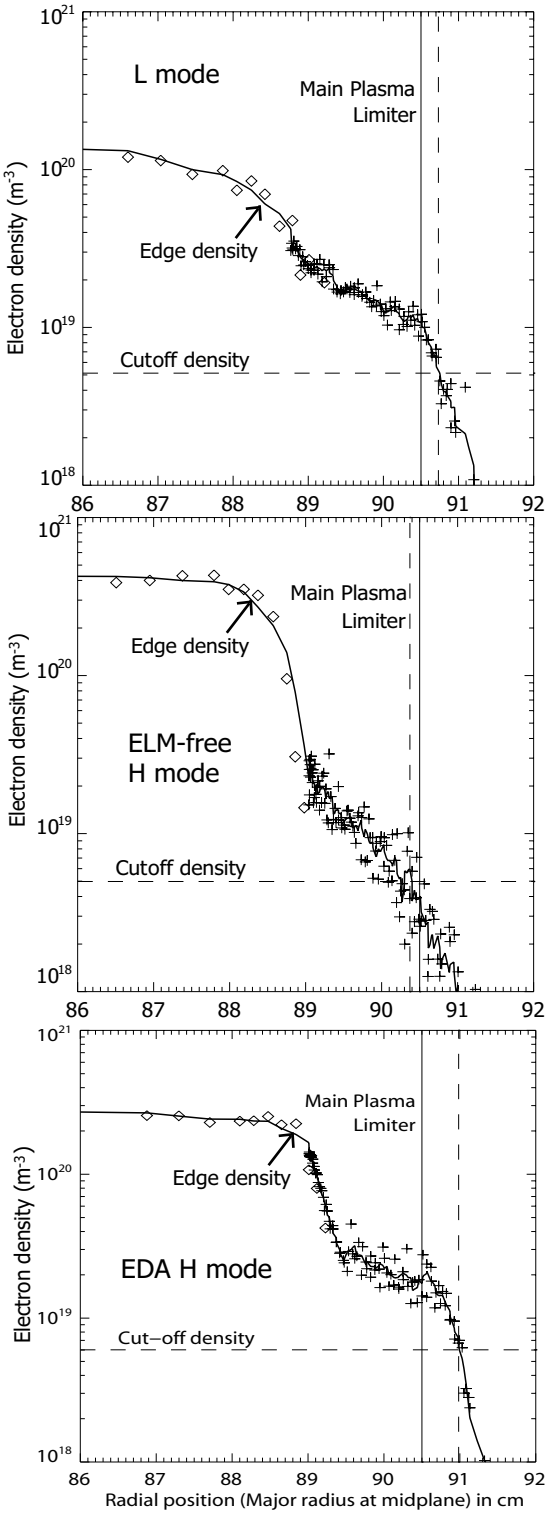

Figure 2. Typical density profiles on Alcator C-Mod measured using Thomson Scattering and Langmuir probes. The cutoff position corresponds to that of the D and E antennas.

JET [Hartmann et al.(2001)] and Tore Supra [M. Goniche and Colas(2003), Clairet(2002)]. The loading resistance depends then strongly upon the outer gap L_g, which is defined as the distance between the main limiter and the Last Closed Flux Surface (LCFS). If the density in the SOL has an exponential decay with a decay length λ_{SOL}, we find $R_L \propto (\frac{n_{LCFS}}{n_{cutoff}})^{2k_{||}\lambda_{SOL}} \exp(-2k_{||}L_g)$. In Tore Supra for example [Clairet(2002)], L_g can vary by $\Delta L_g \sim 6cm$ for different plasmas conditions. With $k_{||} \approx 8m^{-1}$, this leads to a $\sim 70\%$ change in the loading resistance. Tokamaks operating in this regime routinely use gap control to keep L_g low and maintain high coupling to the plasma.

In Alcator C-Mod, the distance to cutoff is not found to be the dominant factor. As can be seen from Figure 2, typical variations in the evanescent length L can be up to $\Delta L \sim 1cm$. With $k_{||} \approx 10m^{-1}$, this gives rise to a $\sim 20\%$ decrease in loading. This is much less than the range found in experiments, as shown in Figure 4 ($\sim 3\Omega$ to $\sim 12\Omega$). In addition, no clear correlation between the loading resistance and the outer gap was observed in Alcator C-Mod. Gap control was also found to be of very limited use. It leads to higher loading resistance only for low density ELM-free H-mode plasmas, as the cutoff layer is expected to move towards the near scrape-off layer.

The different coupling regime observed in C-Mod can be attributed to its operating high density and its compact nature. The cutoff radial position stays very close to the edge of the main plasma limiter and its excursions are small relative to the evanescent decay length of the launched waves. Therefore it does not play such an important role as in Tore Supra or JET, which are larger and lower density devices.

4. Experimental dependence on plasma parameters

As the distance to cutoff is not the dominant factor in Alcator C-Mod, other mechanisms such as the effect of the density gradient (III.B) can be explored to explain the observed variations.

4.1. Dependence on the edge density

The effect of the sharp density profile in the transport barrier region was studied for H-mode plasmas using Thomson scattering data. While the gradient has indeed an effect, a clearer correlation with the loading measurements was found using the density at the top of the pedestal for H-mode plasmas. Figure 3 corresponds to a run day in which this dependence was particularly obvious. The machine was run with a toroidal field of 4.5 T after boronization. The range of neutral pressures at the outer midplane (0.1 - 0.2 mTorr) was small, indicating similar densities in the far SOL. The edge density corresponds to the density at the top of the pedestal in H-mode, and to the density at the last closed flux surface in L-mode, as indicated in Figure 2. Although we show here measurements from D antenna only, the same effect was observed on E- and J-antennas.

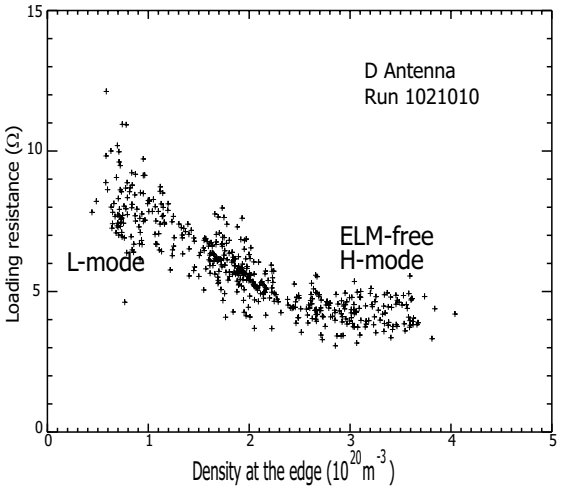

Figure 3. Dependence on the edge density (defined in Fig. 2) for run 1021010.

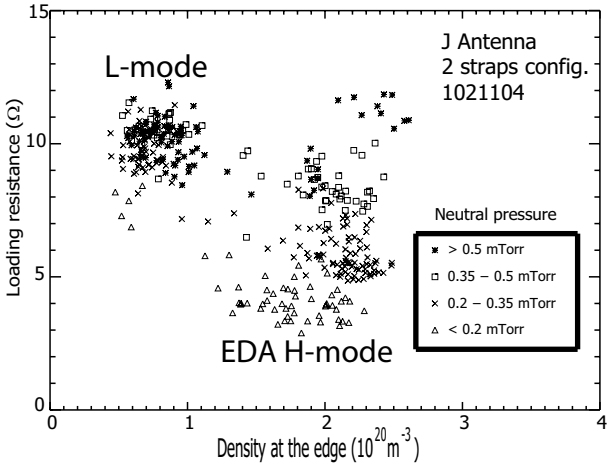

Figure 4. Dependence of the loading resistance on midplane neutral pressure.

4.2. Correlation with the neutral pressure at the midplane

In most discharges, and especially for EDA H-mode plasmas, the measured loading deviates strongly from the trend suggested by the clustering of points in Figure 3. As the neutral pressure becomes higher, the loading resistance can increase signifi cantly. This is illustrated on Figure 4 using loading measurements on J-antenna in a two-strap confi guration, during a typical run day. In Alcator C-Mod, the line average electron density in the SOL is well correlated with the neutral pressure at the outboard midplane [LaBombard et al.(2000)]. Higher neutral pressures indicate therefore higher SOL densities. This suggests that raising the SOL density can increase the antenna loading in H-mode plasmas by a factor of 2, to levels that are similar to typical L-mode phases. Again, this effect is present for all three antennas.

5. 1D Wave propagation model and physical interpretation

These observations suggest that significant variations arise as the shape of the density profile is changed in the propagating region. This cannot be accounted for with a linear density profile model as in Mayberry et al. [Mayberry et al.(1990), Vdovin(1983)]. Here, we followed an approach similar to Ram et al. [Ram and Bers(1984)]. In a slab geometry with the x axis in the radial direction and z in the toroidal direction, the propagation can be described using the ICRF equation [Stix(1992)] in the limit $n_y = 0$:

$$\frac{d^2 E_\perp}{d\xi^2} + K^2(\xi) E_\perp = 0$$

where $K(\xi)^2 = S - n_\parallel^2 - D^2/(S - n_\parallel^2)$ and $\xi = \frac{x\omega}{c}$. $S \equiv R + L$ and $D \equiv R - L$ are the usual Stix parameters [Stix(1992)] (R defined above and $L \equiv 1 - \sum_j \frac{\omega_{pj}^2}{\omega(\omega - \Omega_{cj})}$). S and D are functions of the local density and magnetic field. The origin $\xi = 0$ is taken between the edge region and the Ion Cyclotron resonance layer, away from the two regions, for example at R = 80 cm (major radius). Assuming perfect single pass absorption (outgoing plane wave for $\xi < 0$), we calculate the surface impedance $\frac{E_y}{H_z}$ at the Faraday shield surface (FS), using a fifth order Runge-Kutta algorithm. The power coupled to the plasma is then: $P_{abs} = \frac{1}{2} Re(\int_{FS} \vec{E} \times \vec{H}^* \cdot d\vec{S}) = \frac{1}{2} \int_{FS} Re(\frac{E_\perp}{H_\parallel}) \mid H_\parallel \mid^2 dS$ in this simple geometry. If the self consistent current redistribution on the straps due to the presence of the plasma is ignored, $\mid H_\parallel \mid^2$ is proportional to the square of the input current, and the surface impedance scales with the loading resistance. The proportionality constant accounts for structural properties of the antenna and plasma shape considerations and must be determined for each antenna by comparing the predictions to the experimental data. The same constant was used for the structurally identical D and E antennas in this study. Another parameter dependent on the antenna structure is the radiated $k_\parallel$ spectrum, which was not varied here. Therefore, we only took here into account the $k_\parallel$ component corresponding to the peak radiated power. The effect of other $k_\parallel$ values will be investigated in further studies, with different antenna phasings.

At first, we assumed a flat SOL profile, exponentially decaying beyond the limiter, and with the SOL density proportional to the midplane pressure. Using such a model, the computed values match the observed trends very well in H-mode plasmas: as shown on Figure 5, raising the SOL layer density in the model results in an increase in the predicted loading in H-mode. However, as reported first in [Parisot et al.(2003)], the role of the scrape-off layer density in the L-mode regime is more obscure and the shape of the SOL profile should be taken into account. The actual SOL density profiles were measured using the fast-scanning Langmuir probe during a dedicated run day. The comparison was done for a standard fiducial shape in D(H) L-mode and ELM-free H-mode plasmas. Only 0.5 to 1 MW were injected from the D and E antennas to avoid large heat loads and electrical field pickup. We changed the target line integrated density from $6 \times 10^{19} m^{-2}$ to $1.1 \times 10^{20} m^{-2}$ and the plasma current from 0.8 MA to 1.2 MA. This parameter space corresponds to about 20 discharges, with 3 probe insertions for each. Figure 6 shows the model calculations and the measured loading. As can be seen, good agreement is obtained given the simplicity of the model and experimental

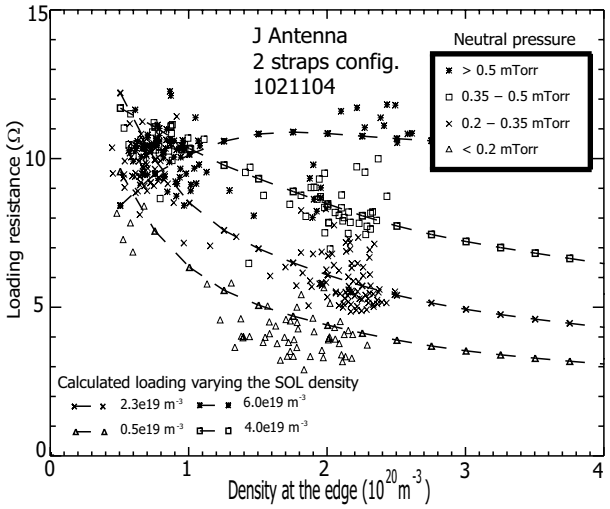

Figure 5. Comparison between experimental data (Figure 4) and model calculations with a flat SOL layer density profile. The increase in the loading with the midplane pressure in H-mode is well reproduced by the model by increasing the SOL density.

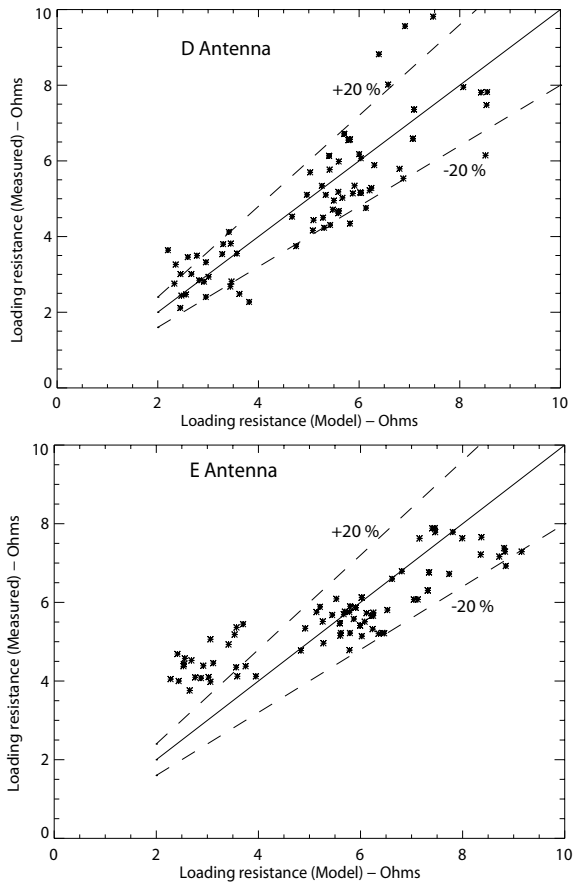

Figure 6. Comparison between modeled and measured loading resistances using experimental density profiles. Good agreement is obtained for both antennas.

uncertainties. However, Figure 6 shows a significant deviation at lower loading. This will be studied in more detail in the next section.

A physical interpretation for this model can be provided as follows. In the regime under consideration, variations due to the exponential term $\exp(-2k_{||}\Delta L)$ are small, i.e. $2k_{||}\Delta L$ is much smaller than 1. Therefore, ICRF loading variations are mainly due to changes in the surface impedance $\frac{E_y}{H_z}$ at the cutoff layer as the shape of the density profile in the propagating region evolves. These changes can be understood in terms of impedance transformation in an inhomogeneous dielectric medium. The characteristic impedance of the plasma is $Z_0(\xi) = \sqrt{\frac{\mu_0}{\epsilon_0}}\frac{1}{K(\xi)}$ and the perpendicular wavelength in the propagating region is $\lambda_\perp(\xi) = \frac{2\pi c}{\omega K(\xi)}$. With the assumption of an outgoing wave towards the plasma core, the inner plasma is modeled as a matched load, which gives an initial condition for the wave impedance $\frac{E_y}{H_z} = Z_0(\xi = 0)$. As $K(\xi) = 0$ at the cutoff layer and then increases with density, $Z_0(\xi = 0)$ is a decreasing function of the density at $\xi = 0$. This contributes to the decrease of the loading resistance with the edge density and would correspond to the evolution of the loading impedance with density if its profile was a step function. As the inhomogeneity in the edge and SOL region is taken into account, this initial value is transformed according to the varying characteristic impedance. For typical density profiles used in Figure 5, the evolution of $Z_0(\xi)$ is illustrated on Figure 7. The radial position has to compared with the local perpendicular wavelengths : we used a wavelength-normalized distance $\int_0^\xi \frac{c}{\omega}\frac{d\xi'}{\lambda_\perp(\xi')}$. We see that the density in the SOL determines both the effective length of the transformer and its mismatch compared to the initial impedance $Z_0(\xi = 0)$. As $Z_0 > Z_0(\xi = 0)$, the profile shape considered here results in a transformation to a higher wave resistance $Re(\frac{E_y}{H_z})$ as the density in the scrape-off layer is increased. The SOL profile has therefore a significant effect on the loading resistance, as seen on Figure 5 for EDA H-mode plasmas. When experimental profiles are considered, which is required especially in L-mode, the transformation becomes less intuitive and the details must be resolved numerically. Note that the model described here will not predict a substantial effect from the SOL region if the cutoff lies in the near-scrape off layer. In addition, for a linear increase in density from below the cutoff density up to a typical edge density, the model presented here predicts an increase in the loading resistance as the slope of transition (density gradient) is decreased, which is consistent with Mayberry et al. [Mayberry et al.(1990), Vdovin(1983)] and could also be interpreted in terms of impedance transformation.

6. Deviations from the model and consequences

In the model above and throughout this paper, we attempt to understand loading variations in terms of global plasma parameters. However this approach has limitations, and the experimental data shows evidence of local behavior. For instance, the D and E antennas are structurally identical and they are operated at very close frequencies (80 MHz and 80.5 MHz), therefore in the same plasma conditions their loading behavior should be very similar. This is indeed found to be correct when considering a large number of discharges. However, for particular discharges, the loading resistance for D antenna can be significantly different from

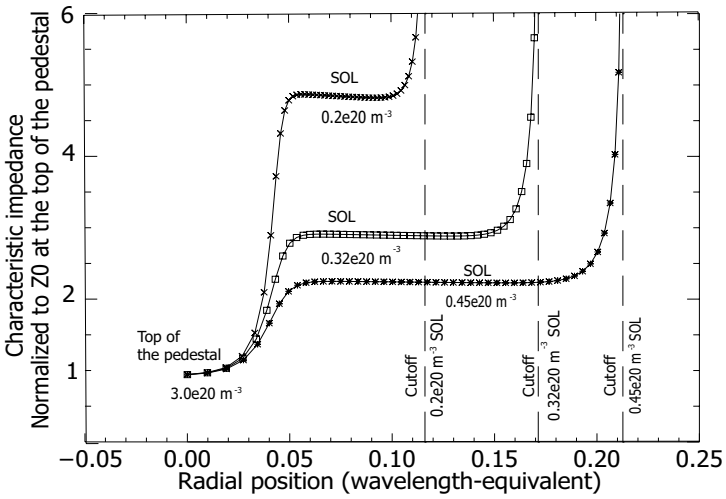

Figure 7. Profiles of the characteristic impedance of the plasma in the edge region, for different SOL densities with a fixed SOL length. The SOL region acts as an impedance transformer, whose characteristic impedance and effective length depends mainly on its density profile.

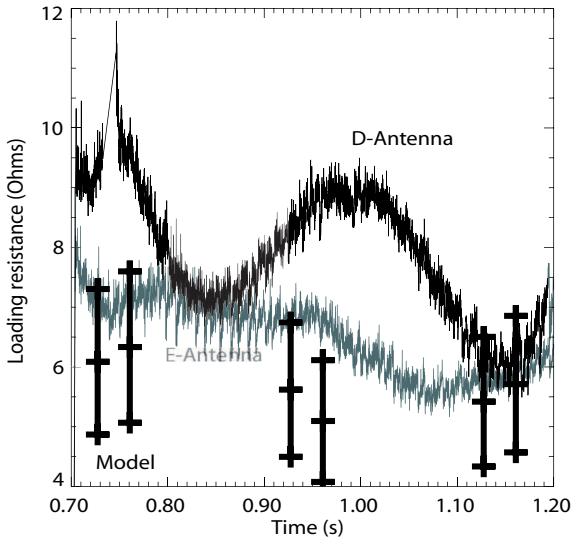

Figure 8. Loading behavior of the structurally identical D and E antennas in a particular discharge. The observed difference cannot be explained in terms of global plasma parameters.

that of E antenna. In Figure 8, the variations in the loading resistance for the D and E antenna are signifi cantly different. This is apparently local behavior as it cannot be explained in terms of global parameters and can last for a signifi cant fraction of the RF pulse. The discharges where the predicted and measured loading resistance were in disagreement on Figure 6 exhibit similar differences in the time evolution of the loading for the D and E antennas.

Several mechanisms could be invoked to explain the local loading behavior. Density injections or convective cells [Myra et al.(1995)] could change the density profi le locally. However, the D and E antennas use boron nitride limiter tiles, which are expected to limit these effects. Alternatively, part of the radiated spectrum could be coupled to surface waves

or slow waves. In such case, strong edge absorption is expected. The approach highlighted in this paper could be significantly improved by measuring the density profile local to the antenna. This has been done using reflectometry on TFTR, DIII-D [Hanson et al.(1995)] and NSTX [Wilgen(2001)] for example.

ICRF antenna-plasma coupling codes for loading predictions include the basic cold plasma physics used here, and therefore they will reproduce the behavior reported here. However, our results suggest that a precise knowledge of the local density profiles at the edge is critical for accurate predictions in this regime. Diagnostic limitations or difficulties in predicting density profiles for future devices must therefore be taken into account when evaluating and benchmarking ICRF loading calculations. Scaling analysis or simple semi-empirical models could be helpful to capture and understand the dominant effects of changes in the plasma parameters in many different regimes using a large database. Robust antenna-plasma coupling codes, which usually require lengthy computation, could then be expected to reproduce the semi-empirical dependence quantitatively from a full 3D model of the antenna structure and antenna-plasma interactions. This benchmarking process should involve studies from tokamaks with different coupling regimes. As shown in this work, Alcator C-Mod offers a unique opportunity to study effects which are not dominant on other tokamak devices and may be relevant for next step tokamak experiments.

For instance, taking prospective parameters as in [M. Goniche and Colas(2003)], the cutoff density in ITER will be rather low $n_{e,cutoff} \sim 0.5 - 1.6 \times 10^{18} m^{-3}$ compared to the typical edge densities. This is due in particular to the low value of the peak $k_{||} \sim 4m^{-1}$. The cutoff surface should therefore lie in the far scrape-off layer and this may lead to similar effects as in C-Mod. In addition, the changes in the evanescent length ΔL may be significant given the size of the machine, although the low $k_{||}$ value will not lead to higher values of the factor $2k_{||}\Delta L$ than that seen in JET, Tore Supra or DIII-D. More detailled simulations would be required to determine the relative role of these effects in terms of loading variations.

7. Conclusions

Compared to other ICRF loading studies on JET or Tore Supra, a different dependence on plasma parameters for the loading resistance is found on Alcator C-Mod. Due to the high electron density at the edge, the evanescent length is short and experiences only limited changes. Therefore it does not dominate the loading variations. The role of other mechanisms, such as the effect of the edge density profile, can therefore be studied directly. Experimental measurements on three separate antennas show a strong correlation between the loading resistance and the shape of the density profile in the propagating region beyond the cutoff layer. For instance, in EDA H-mode, a higher density in the scrape-off layer increases the coupling to a similar level as for L-mode plasmas. The observed behavior in L-mode, ELM-free H-mode and EDA H-mode can be reproduced with numerical calculations of wave propagation in an inhomogeneous slab and interpreted in terms of impedance transformation in the SOL region. A major limitation of this approach is the presence of local behavior in front of each antenna. Further studies of these effects would requires density profile

measurements local to the antennas. These diagnostic limitations and fine density profile effects should be taken into account in more advanced modeling efforts.

Acknowledgments

The authors would like to thank the Alcator C-Mod team for its help in running the tokamak and obtaining these results. This work is supported by Department of Energy Coop. Agreement DE-FC02-99ER54512.

References

[Porkolab et al.(1998)] M. Porkolab et al., Plasma Physics and Controlled Fusion **40**, A35 (1998).
[Kaye(94)] A. Kaye, Fusion Engineering and Design **24** (94).
[M. Goniche and Colas(2003)] S. B. M. Goniche and L. Colas, Nucl. Fusion pp. 92–106 (2003).
[Pinsker(1998)] R. Pinsker, Tech. Rep., General Atomics (1998).
[Carter et al.(1996)] M. Carter et al., Nucl. Fusion **36**, 209 (1996).
[Pécoul et al.(1998)] S. Pécoul et al., in *Proc. 27th Eur. Conf. on Fusion and Plasma Physics, Budapest* (1998), p. 388.
[Maggiora et al.(2003)] R. Maggiora et al., in *15th Top. Conf. on RF Power in Plasmas, Moran* (American Institute of Physics, New York, 2003), vol. 694 of *AIP Conference Proceedings*, p. 134.
[Mayberry et al.(1990)] M. Mayberry et al., Nuclear Fusion **30**, 579 (1990).
[Hartmann et al.(2001)] D. Hartmann et al., in *14th Top. Conf. on RF power in plasmas, Oxnard* (American Insitute of Physics, New York, 2001).
[Clairet(2002)] F. Clairet, in *29th EPS conf. on. Plasma Phys. and Contr. Fusion, Montreux* (2002), vol. ECA Vol 26B P-1.607.
[Wukitch et al.(2002)] S. Wukitch et al., in *19th Fusion Energy Conference, Lyon, France* (2002), IAEA FT/P1-14.
[Hughes et al.(2001)] J. Hughes et al., Review of Scientific Instruments **72**, 1107 (2001).
[Hughes et al.(2003)] J. Hughes et al., Review of Scientific Instruments **74**, 1667 (2003).
[Greenwald et al.(1999)] M. Greenwald et al., Phys. of plasmas **6**, 1943 (1999).
[Stix(1992)] T. H. Stix, *Waves in plasma* (AIP, 1992).
[Vdovin(1983)] V. Vdovin, Nuclear Fusion **23**, 1435 (1983).
[LaBombard et al.(2000)] B. LaBombard et al., Nucl. Fusion **40**, 2041 (2000).
[Ram and Bers(1984)] A. Ram and A. Bers, Nucl. Fusion **24**, 679 (1984).
[Parisot et al.(2003)] A. Parisot et al., in *15th Topical Conference on RF Power in plasmas, Moran* (American Institute of Physics, New York, 2003), vol. 694 of *AIP conference proceedings*, p. 158.
[Myra et al.(1995)] J. Myra et al., Phys. of plasmas **3**, 699 (1995).
[Hanson et al.(1995)] G. Hanson et al., in *11th Top. Conf. on RF Power in Plasmas* (American Institute of Physics, New York, 1995), vol. 355 of *AIP Conference Proceedings*, p. 463.
[Wilgen(2001)] J. Wilgen, in *APS-DPP Meeting, Long Beach, CA* (2001).